멤브레인(Membrane Journal)
Vol. 34 No. 5 October 2024, 262-271

Print ISSN: 1226-0088
Online ISSN: 2288-7253
DOI: https://doi.org/10.14579/MEMBRANE_JOURNAL.2024.34.5.262

산화 그래핀의 이산화탄소 흡착 거동

박 인 호 · 박 호 범†

한양대학교 에너지공학과
(2024년 10월 10일 접수, 2024년 10월 17일 수정, 2024년 10월 18일 채택)

On the Carbon Dioxide Sorption of Graphene Oxide

Inho Park and Ho Bum Park†

Department of Energy Engineering, Hanyang University, Seoul 04763, Republic of Korea
(Received October 10, 2024, Revised October 17, 2024, Accepted October 18, 2024)

요 약: 비록 산화 그래핀의 비표면적은 환원된 산화 그래핀에 비해 낮지만, 산화 그래핀의 이산화탄소 흡착량은 기존 그래핀 또는 환원된 산화 그래핀에 비해 많다. Lerf-Klinowski 모델에 따르면, 산화 그래핀은 가장 자리와 면 내부에 수산화기, 에폭시드, 카보닐, 카복실기 등이 있으며, 이러한 작용기가 이산화탄소 분자와 강하게 결합하여 화학 흡착을 유도한다. 본 연구에서는 산소 플라즈마/UV 오존 및 열처리를 통해 그래핀 산화물의 산소 함량과 이산화탄소 흡착 친화도 사이의 상관관계를 탐구하였다. 산소 함량의 변화는 XPS와 FT-IR 분석을 통해 확인하였다. 흥미롭게도 산화 그래핀의 이산화탄소 흡착 경향은 전체 산소 함량과 정비례하지 않았다. 반면, XPS 분석 결과 산화 그래핀의 카보닐 작용기가 이산화탄소 흡착에 중요한 기여를 하는 것으로 나타났다. 이러한 연구 결과는 산화 그래핀의 특성 및 이를 활용한 탄소 포집 및 가스 저장 응용 가능성에 대한 통찰을 제공한다.

Abstract: Although the surface area of graphene oxide (GO) is lower than that of reduced graphene oxide (rGO), the amount of carbon dioxide adsorbed on GO is higher compared to graphene or rGO. According to the Lerf-Klinowski model, GO contains hydroxyl, epoxide, carbonyl, and carboxyl groups on its edges and basal planes, which strongly bind carbon dioxide molecules, even leading to chemisorption. In this study, we explored the correlation between carbon dioxide sorption affinity and oxygen content in GO by applying oxygen plasma/UV ozone and thermal treatments. The variation in oxygen content was confirmed using XPS and FT-IR analysis. Interestingly, the trend of carbon dioxide sorption in GO was not directly proportional to the overall oxygen content. XPS peak analysis revealed that carbonyl groups significantly contribute to carbon dioxide sorption. These findings provide insight into the intrinsic properties of GO and its potential applications in carbon capture and gas storage.

Keywords: *GO, carbon dioxide, sorption, membrane, gas separation*

1. Introduction

Graphene is a single-atom-thick sheet of sp^2 hybridized carbon atoms arranged in a hexagonal lattice. Since its experimental discovery in 2004[2], various methods have been developed to synthesize graphene and its derivatives. For instance, large-area, single-layer graphene can be synthesized on transition metals using the chemical vapor deposition (CVD) method[3]. Alternatively, graphene oxide (GO) and reduced (rGO) are produced through chemical exfoliation of natural graphite[4-6], a method that is effective for large-scale production. These graphene-like materials are utilized in applications such as electronic devices, hydrogen storage, and carbon capture[7-10].

†Corresponding author(e-mail: badtzhb@hanyang.ac.kr; http://orcid.org/0000-0002-8003-9698)

GO is highly soluble in water and various organic solvents[11] due to the hydrophilicity induced by oxygen functional groups present on its basal planes and edges. Despite extensive research, knowledge about the atomic structure and physical properties of GO remains limited. Several models have been proposed to describe the structural features of GO, including those by Hofmann[12], Ruess[13], Scholz-Boehm[14], Nakajima-Matsuo[15], and Lerf-Klinowski[1]. The widely accepted Lerf-Klinowski model suggests that GO contains epoxy and hydroxyl groups bonded on the basal planes, with carboxyl groups functionalized at the edges. While the interlayer spacing of graphite is 0.34 nm, oxidation disrupts the sp^2 hybridized carbon-carbon aromatic rings due to the action of oxygen-containing acids. As a result, the incorporation of functionalized oxygen groups expands the interlayer spacing of GO to approximately 0.8~0.9 nm.

One potential application of GO (GO) is gas storage and carbon dioxide capture. To function effectively as an absorbent, a material should have high porosity, a large surface area, and specific functional groups that preferentially interact with the target gas. Recently, three-dimensional metal-organic frameworks (MOFs), composed of metal oxide clusters, have demonstrated large internal surface areas and have shown great promise in gas adsorption and storage[16,17]. Studies have indicated that carbon dioxide binds more stably to carboxylic acid and hydroxyl groups compared to other functional groups[18-20]. Given that GO contains these carboxylic acid and hydroxyl groups and also has a high surface area, it is well-suited for carbon dioxide absorption.

In this study, we synthesized GO sheets using the modified Hummers' method[4] and evaluated their gas sorption properties with nitrogen, hydrogen, and carbon dioxide. We assessed the sorption affinity of GO for carbon dioxide under both low- and high-pressure conditions. We hypothesized that the oxygen functional groups in GO play a crucial role in its interaction with carbon dioxide, and that increasing the oxygen content on the basal plane or edges of GO would enhance its carbon dioxide sorption capacity. To manipulate the oxygen content, we used oxygen plasma and UV ozone treatments, which are known to introduce unstable oxygen radicals that break the sp^2 carbon-carbon rings, forming carboxyl, carbonyl, and hydroxyl groups [21]. Additionally, thermal treatment was employed to reduce the oxygen content by removing these functional groups[22].

The variations in oxygen content were confirmed using X-ray photoelectron spectroscopy (XPS) and Fourier transform infrared spectroscopy (FT-IR). Contrary to our expectations, the carbon dioxide sorption measurements revealed that the amount of CO_2 adsorbed was not directly proportional to the oxygen content. We hypothesize that specific oxygen functional groups are primarily responsible for strong CO_2 binding. Through multi-peak analysis using XPS, we examined the changes in various oxygen groups to identify those most critical for carbon dioxide sorption.

2. Experimental Section

2.1. Synthesis of GO

Synthetic graphite powder (SP-1, fine grade) was supplied by Bay Carbon Inc. (Bay City, MI, USA) and used without further purification. All other reagents, including sulfuric acid (H_2SO_4, 97%), hydrochloric acid (HCl, 37% in water), hydrogen peroxide (H_2O_2, 50% in water) from Aldrich Chemical Co. (Milwaukee, WI, USA), and $KMnO_4$ from JUNSEI Chemical Co. (Tokyo, Japan), were of analytical grade and used as received.

GO was synthesized using the modified Hummers method[6]. Graphite powder was oxidized with $KMnO_4$ in concentrated sulfuric acid. After oxidation, the solution was treated with a mixture of hydrogen peroxide and deionized water. The suspension was then filtered and washed with a 1 M hydrochloric acid solution and deionized water. The resulting colloidal suspension was separated by centrifugation and dried under vacuum.

2.2. Physical sorption measurement (BET, high-pressure sorption)

Nitrogen gas adsorption isotherms were measured at 77 K, and carbon dioxide measurements were conducted at 273.15 K using a surface area and porosimetry analyzer (ASAP 2020, Micromeritics Instrument Corp., Norcross, GA, USA). The gas sorption technique was based on the Brunauer-Emmett-Teller (BET) method and the Horvath-Kawazoe method. Samples were placed in the sample chamber and subjected to vacuum overnight at 60°C to remove any gas impurities. The dried sample weight was then used to determine the specific adsorption of nitrogen, hydrogen, and carbon dioxide.

High-pressure sorption was conducted using the manometric method[23], which measures the pressure or volume of gas adsorbed or desorbed from the sample at equilibrium with the gas at a set temperature. The equipment includes two isolated chambers (V_1, V_2). After placing the sample in V_2, both chambers were degassed for 12 hours, and gas was introduced into V_1 at a set pressure. When the valve between the two chambers was briefly opened and then closed, the pressure in both chambers equalized, but over time, the pressure in V_2 decreased as the gas was adsorbed until equilibrium was reached. The adsorbed gas amount was calculated based on the difference between the initial and equilibrium pressures in V_2.

2.3. Chemical sorption measurement (pulse chemisorption, double isotherm method)

Carbon dioxide pulse chemisorption was performed using an Autochem II 2920 chemisorption analyzer (Micromeritics). Approximately 200 mg of GO powder was placed in a quartz reactor. Before the pulse chemisorption measurement, the GO powder was degassed under vacuum at 80°C for 24 hours, and then purged with He (99.999%, 50.21 cm^3 (STP)/min). CO_2 pulses (0.54 cm^3) were flowed through the sample for 2 minutes.

The double isotherm method was conducted using the ASAP 2020 porosimetry analyzer (Micromeritics Instrument Corp., Norcross, GA, USA). The GO powder was degassed at 80°C for 24 hours before measurement. The first isotherm provided the total volume of adsorbed carbon dioxide. Subsequently, the weakly adsorbed CO_2 was evacuated before the second measurement. The chemical sorption amount of CO_2 was calculated as the difference between the total and weakly adsorbed CO_2.

2.4. Thermal annealing, UVO treatment, and O_2 plasma treatment

GO powder was treated using a UVO system (Ozone Cure 16, Minuta Technology) with various exposure times (30 min, 60 min). The equipment emitted UV light at 185 nm and 254 nm, with the GO positioned 2 cm from the UV source. Oxygen plasma treatment was also conducted using an oxygen plasma system (JPH-1000, A.P.P. Co., Ltd.), with an Ar/O_2 mixture flow rate of 8 L/min and 10 L/min, respectively, for different exposure times (30 s, 60 s).

2.5. X-ray photoelectron spectroscopy (XPS)

XPS analysis was performed using a monochromatic Al Kα radiation source (1486.6 eV) (QUANTUM 2000, Physical Electronics) to determine changes in the atomic ratios of carbon to oxygen and to identify functional groups.

2.6. Fourier transform infrared spectroscopy (FT-IR)

FT-IR analysis was conducted using an IlluminatIR infrared microspectrometer (SensIR Technologies, Danbury, CT, USA) in the range of 4000~500 cm^{-1} to study the chemical structure. KBr pellet samples were prepared with a sample-to-KBr ratio of 1:500 by weight. The KBr pellet was dried overnight in a vacuum oven, and FT-IR spectra were recorded after complete drying. A total of 64 scans were performed with a resolution of 4 cm^{-1}.

3. Results and Discussion

3.1. Nitrogen adsorption isotherms in GO and RGO

GO (GO) was synthesized using the modified Hummers method, and rGO (rGO) was produced using hydrazine. During the conversion of GO to rGO, the oxygen functional groups on the basal plane and edges are removed. Fig. 1(a) presents typical nitrogen adsorption and desorption curves for both GO and rGO, showing surface areas of 62.5 m^2/g and 74 m^2/g, respectively. The higher surface area of rGO is attributed to structural defects on the basal plane, which increase the number of sorption sites. The hysteresis observed in both GO and rGO is characteristic of type IV isotherms[24], indicating mesoporous absorbents. Fig. 1(b) shows that the average pore diameter for both GO and rGO is around 4 nm.

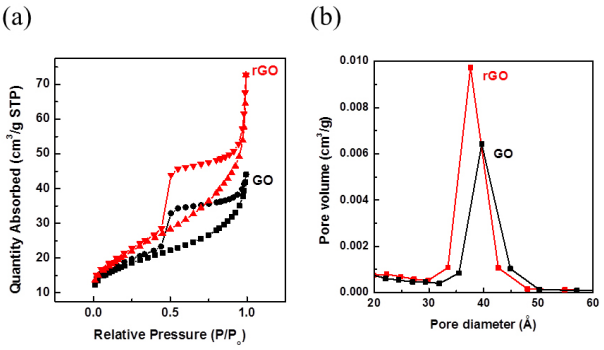

Fig. 1. Nitrogen isotherm of GO and rGO and their pore sizes.

3.2. Carbon dioxide adsorption isotherms in GO and RGO

Unlike the nitrogen adsorption isotherm, GO exhibits a higher carbon dioxide adsorption capacity than rGO. Fig. 2 displays the CO_2 and hydrogen sorption isotherms for GO and rGO at low pressure. The hydrogen adsorption isotherms for both GO and rGO increase rapidly with relative pressure up to 0.1, followed by a linear increase. GO adsorbs slightly more hydrogen than rGO. Interestingly, the amount of CO_2 adsorbed by GO is not only higher than hydrogen but also significantly greater than that of rGO, indicating a preference for CO_2 adsorption in GO. At higher pressures, from 25 to 500 psi (Fig. 3), GO continues to exhibit higher CO_2 adsorption than hydrogen. The oxygen-containing functional groups (e.g., O–H, C–O–C, C=O, O–C=O, and COOH) present in GO enhance binding energies and charge transfer, promoting CO_2 adsorption on the basal planes and edges and even facilitating chemisorption.

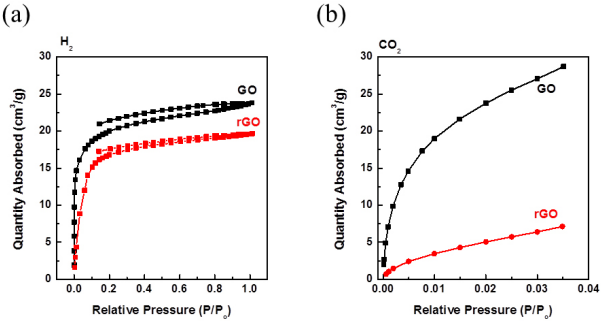

Fig. 2. Hydrogen and carbon dioxide isotherm in GO and rGO.

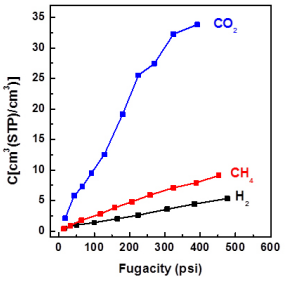

Fig. 3. High pressure hydrogen and carbon dioxide sorption isotherm measurement of GO.

3.3. Chemical sorption measurement

Fig. 4(a) illustrates the cumulative CO_2 adsorption based on the TCD signal area as a function of pulse

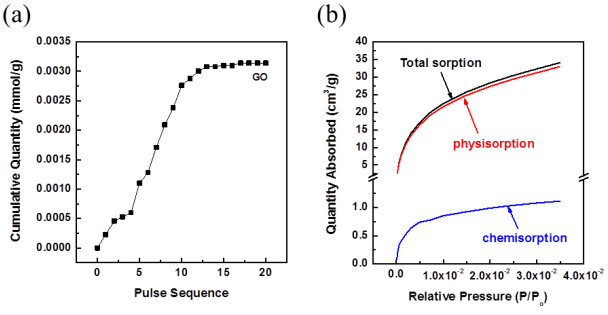

Fig. 4. Carbon dioxide pulse chemisorption measurement and double chemisorption measurement.

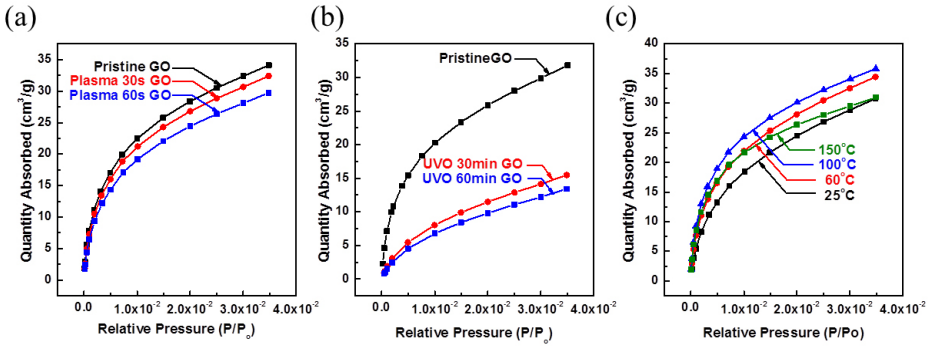

Fig. 5. Carbon dioxide sorption isotherm of GO treated oxygen plasma/UV ozone and thermal.

number during CO_2 pulse chemisorption at room temperature. In the initial pulse, a significant amount of CO_2 is adsorbed by GO, and as the number of pulses increases, the peak area stabilizes as the adsorption sites become saturated. Once the chemical sorption sites are saturated, further CO_2 adsorption becomes difficult.

A static volumetric double isotherm method at 273.15 K was used to measure CO_2 chemisorption (Fig. 4(b)). The first isotherm indicates the total amount of chemisorbed CO_2, while the second represents the reversible physisorbed CO_2. The difference between the two gives the amount of irreversible chemisorption.

3.4. Carbon dioxide adsorption in GO under oxygen plasma/UVO and thermal treatment

To enhance oxygen content and CO_2 sorption sites, GO was treated with UV ozone and oxygen plasma for varying durations. These treatments introduce oxygen radicals that functionalize atomic defects and break carbon rings, promoting the formation of oxygen-containing groups such as C–O, C=O, and O–C=O. It was anticipated that increasing oxygen content would correspond to more CO_2 sorption sites, but this was not the case.

Figs. 5(a) and (b) show the low-pressure CO_2 isotherms for UV ozone and oxygen plasma-treated GO. The CO_2 adsorption amount decreases with increasing treatment duration. Pristine GO adsorbs 1.5 cm^3/g of CO_2, while oxygen plasma-treated GO adsorbs 1.4 cm^3/g (30 s) and 1.3 cm^3/g (60 s). UV ozone-treated GO adsorbs 0.7 cm^3/g (30 min) and 0.6 cm^3/g (60 min). These results indicate that CO_2 adsorption is not proportional to oxygen content. To further investigate, thermal treatment was used to reduce carbon content, showing a correlation between decreased carbon content and reduced CO_2 sorption.

Thermogravimetric analysis (TGA) revealed that at around 130°C, carbon monoxide and carbon dioxide are released from oxygen-containing functional groups. This suggests that oxygen content in GO decreases as temperature increases. Fig. 5(c) shows that CO_2 adsorption increases with temperature up to a point, after which it decreases beyond 150°C as GO becomes deoxygenated. This indicates that sufficient oxygen groups are necessary for effective CO_2 sorption, highlighting that specific oxygen functional groups play a crucial role.

3.5. XPS analysis

Chemically synthesized GO and modified GO, subjected to various treatments, exhibit several distinct carbon-oxygen functional groups on their basal planes and edges. These groups were characterized using x-ray photoelectron spectroscopy (XPS). The XPS peaks were fitted using Gaussian and Lorentzian distributions after background subtraction. The XPS results for pristine GO, as shown in Fig. 7(a), reveal different oxygen group contents. The peak at 284.6 eV corresponds to the sp^2 orbital of the C=C bond, while the peak at 286.5 eV is associated with the epoxide

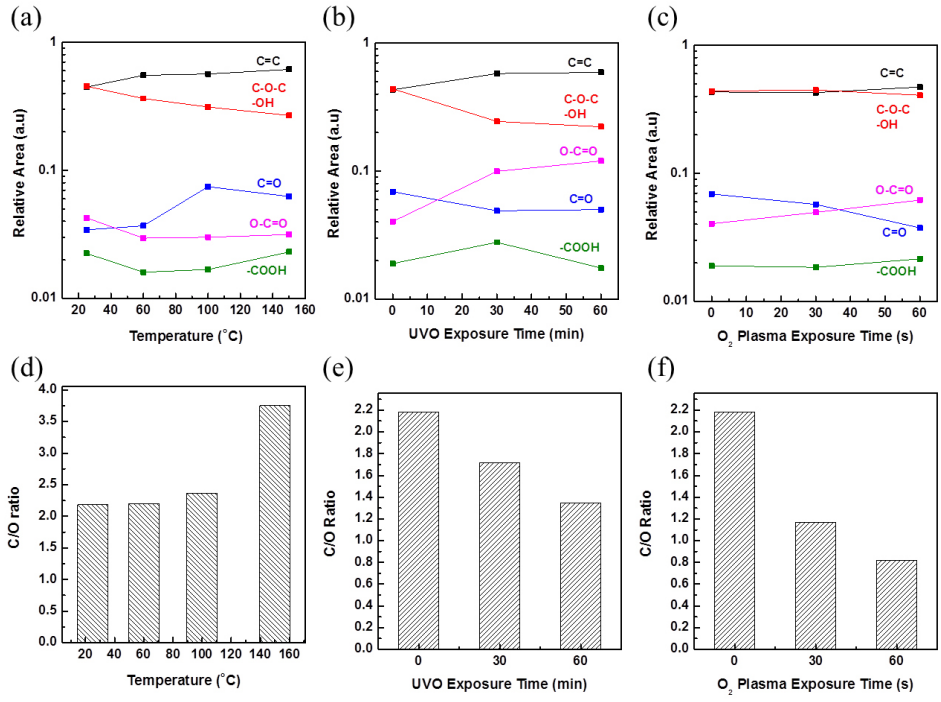

Fig. 6. Variation of oxygen groups and carbon contents of oxygen plasma/UV ozone and thermal treated GO.

group and carbon atoms bonded to oxygen in hydroxyl configurations (O–H/C–O–C). Additional peaks include the carbonyl group (C=O) at 287.8 eV, O–C=O groups at 288.5 eV, and COOH groups at 289.3 eV. The peak at 290.2 eV is attributed to the $\pi-\pi^*$ transition of delocalized electrons in the valence band.

The primary bonding configuration of carbon atoms in GO is the C=C bond, which forms the hexagonal rings typical of graphite. Other oxygen groups are bonded to sp^2 and sp^3 hybridized carbon atoms, such as the epoxy and hydroxyl groups on the basal plane and the carboxyl group at the edges. With increased plasma treatment time, the sp^3 hybridized epoxy and hydroxyl groups (286.5 eV) on the basal plane and the carbonyl groups (287.8 eV) decrease, while the O–C=O groups (288.5 eV) increase. The COOH group (289.3 eV) shows little to no change.

The carbon/oxygen ratio for pristine GO, as shown in Fig. 6(d), was calculated by dividing the area under the C 1s peak by that of the O1s peak and adjusting by the photo-ionization cross-section ratio, yielding a value of 2.2. After oxygen plasma treatment, the carbon/oxygen ratio dropped to 1.2 for the 30-second treatment and to 0.8 for the 60-second treatment. Similarly, UV ozone treatment for 30 and 60 minutes resulted in ratios of 1.7 and 1.3, respectively. Figs. 6(a), (b), and (c) illustrate changes in the relative percentages of each oxygen group. The oxygen content, as shown in Figs. 6(d), (e), and (f), slightly increases with both oxygen plasma and UV ozone treatments, while the sp^2 carbon bond (284.6 eV) decreases due to functionalization by oxygen radicals. The peak intensity of the C–O–C/O–H groups (286.5 eV) and the C=O group (287.8 eV) decreases, whereas the O–C=O group (288.5 eV) relatively increases. The COOH group (289.3 eV) shows slight changes or remains stable over time. In contrast, for thermally treated GO, the peak intensities of the C–O–C/O–H groups (286.5 eV), O–C=O group (288.5 eV), and COOH group (289.3 eV) decrease, while the C=O group (287.8 eV) increases with rising temperature, as shown in Figs. 7 and 8.

3.6. FT-IR analysis

FT-IR analysis was performed to confirm the func-

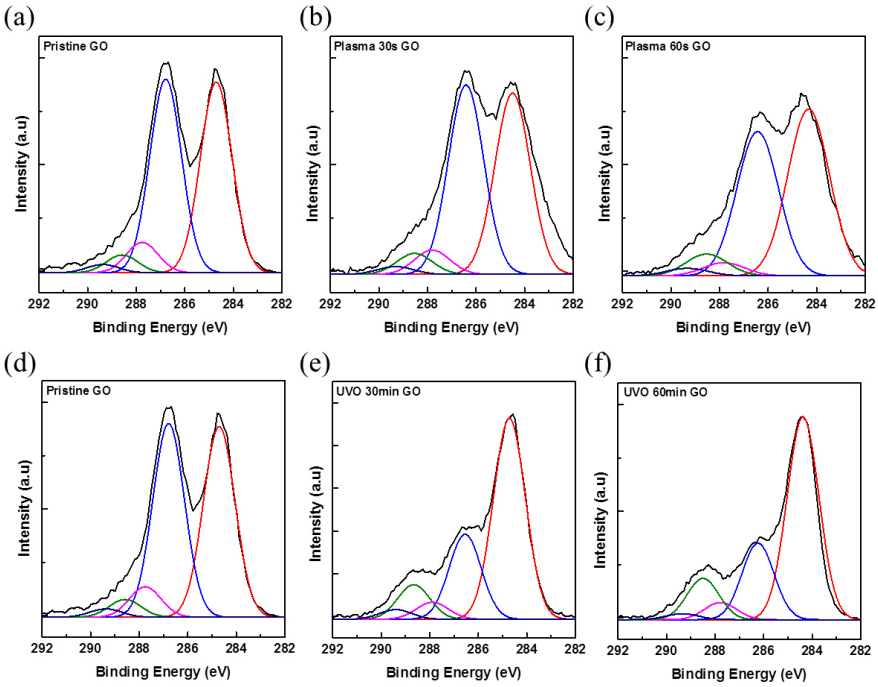

Fig. 7. C 1s spectra of oxygen plasma/UV ozone treated GO.

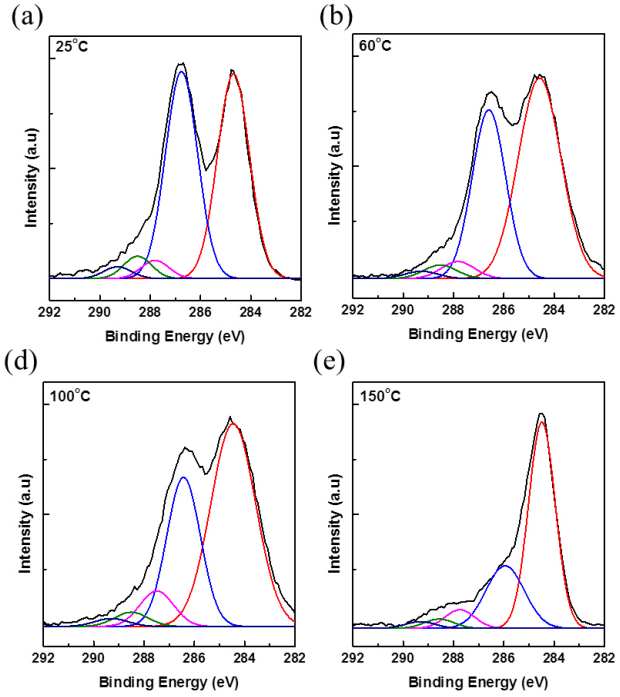

Fig. 8. C 1s spectra of thermal treated GO.

tional groups present in GO after oxygen plasma, UV ozone, and thermal treatments (Fig. 9). In pristine GO, O–H stretching (3000~3400 cm^{-1}), C=C (1570 cm^{-1}), C=O (1720 cm^{-1}), C–O (epoxy at 1230 cm^{-1}), and C–

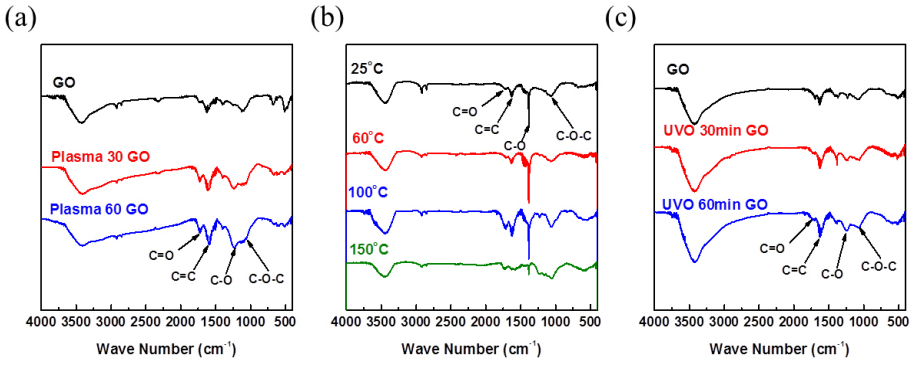

Fig. 9. FT-IR spectra of oxygen plasma/UV ozone and thermal treated GO.

O (alkoxy at 1060 cm^{-1}) vibrations were observed[25]. With increasing oxygen plasma and UV ozone exposure, the intensity of the C=O group at 1720 cm^{-1} and O–H group decreases, while the C–O group intensity increases. For thermally treated GO, the C=O and C–O–C group intensities increase, corresponding with XPS findings.

4. Conclusions

Understanding the intrinsic properties of GO is crucial for its various applications. In this study, we explored the gas sorption capabilities of chemically synthesized GO and rGO. Nitrogen sorption measurements revealed the presence of narrow mesopores, and despite its lower surface area compared to rGO (as measured by nitrogen adsorption), GO exhibited a higher carbon dioxide sorption capacity. The carbon-oxygen functional groups in GO provide active sites for carbon dioxide adsorption, leading to even chemisorption.

To enhance the carbon dioxide sorption affinity, we increased the oxygen content using oxygen plasma and UV ozone treatments for different durations. Contrary to expectations, the carbon dioxide sorption amount decreased. However, carbon dioxide sorption increased with higher thermal treatment temperatures. During oxygen plasma and UV ozone treatments, the sp^2 network of the C=C rings was disrupted, increasing the concentration of O–C=O groups while decreasing the C=O groups. In contrast, thermal treatment led to an increase in C=O groups as the temperature rose. These variations in C=O group concentrations were further confirmed using FT-IR analysis for both oxygen plasma/UV ozone and thermal treatments.

Our results indicate that the amount of carbon dioxide sorption is closely related to the presence of C=O groups, which interact more stably with CO_2 than other oxygen functional groups.

Acknowledgement

This work was supported by the Materials & Components Technology Development Program (Project number: 20011497) funded by the Ministry of Trade, Industry, & Energy (MOTIE, Korea).

Reference

1. A. Lerf, H. He, M. Forster, and J. Klinowski, “Structure of graphite oxide revisited”, *J. Phys. Chem. B.*, **102**, 4477-4482 (1998).
2. K. Novoselov, A. K. Geim, S. V. Morozov, D. Jiang, Y. Zhang, S. V. Dubonos, I. V. Grigorieva, and A. A. Firsov, “Electric field effect in atomically thin carbon films”, *Science*, **306**, 666-669 (2004).
3. K. S. Kim, Y. Zhao, H. Jang, S. Y. Lee, J. M. Kim, K. S. Kim, J. H. Ahn, P. Kim, J. Y. Choi, and B. H. Hong, “Large-scale pattern growth of graphene films for stretchable transparent electro-

des", *Nature*, **457**, 706-710 (2009).
4. W. S. Hummers Jr. and R. E. Offeman, "Preparation of graphitic oxide", *J. Am. Chem. Soc.*, **80**, 1339-1339 (1958).
5. D. A. Dikin, S. Stankovich, E. J. Zimney, R. D. Piner, G. H. B. Dommett, G. Evmenenko, S. T. Nguyen, and R. S. Ruoff, "Preparation and characterization of GO paper", *Nature*, **448**, 457-460 (2007).
6. S. Stankovich, D. A. Dikin, R. D. Piner, K. A. Kohlhaas, A. Kleinhammes, Y. Jia, Y. Wu, S. T. Nguyen, and R. S. Ruoff, "Synthesis of graphene-based nanosheets via chemical reduction of exfoliated graphite oxide", *Carbon*, **45**, 1558-1565 (2007).
7. G. Srinivas, J. W. Burress, J. Ford, and T. Yildirim, "Porous GO frameworks: Synthesis and gas sorption properties", *J. Mater. Chem.*, **21**, 11323-11329 (2011).
8. J. W. Burress, S. Gadipelli, J. Ford, J. M. Simmons, G. Srinivas, and T. Yildirim, "GO framework materials: Theoretical predictions and experimental results", *Angew. Chem. Int. Ed.*, **49**, 8902-8904 (2010).
9. G. Srinivas, J. W. Burress, T. Yildirim, and M. R. Hartman, "Synthesis of graphene-like nanosheets and their hydrogen adsorption capacity", *Carbon*, **48**, 630-635 (2010).
10. A. Ghosh, K. S. Subrahmanyam, K. S. Krishna, S. Datta, A. Govindaraj, S. K. Pati, and C. N. R. Rao, "Uptake of H_2 and CO_2 by graphene", *J. Phys. Chem. C*, **112**, 15704-15707 (2008).
11. J. Paredes, S. Villar-Rodil, A. Martinez-Alonso, and J. Tascon, "GO dispersions in organic solvents", *Langmuir*, **24**, 10560-10564 (2008).
12. U. Hofmann and R. Holst, "The acid nature and methylation of graphitic oxide", *Ber. Dtsch. Chem. Ges. B.*, **72**, 754-771 (1939).
13. G. Ruess, "Über das graphitoxyhydroxyd (graphitoxyd)", *Monatsh. Chem.*, **76**, 381-417 (1946).
14. W. Scholz and H. B. Boehm, "Untersuchungen am Graphitoxid. VI. Betrachtungen zur Struktur des Graphitoxids", *Z. Anorg. Allg. Chem.*, **369**, 327-340 (1969).
15. T. Nakajima, A. Mabuchi, R. Hagiwara, N. Watanabe, and F. Nakamura, "Discharge characteristics of graphite fluoride prepared via graphite oxide", *J. Electrochem. Soc.*, **135**, 273-277 (1988).
16. M. E. Davis, "Ordered porous materials for emerging applications", *Nature*, **417**, 813-821 (2002).
17. R. Banerjee, A. Phan, B. Wang, C. Knobler, H. Furukawa, M. O'Keeffe, and O. M. Yaghi, "High-throughput synthesis of zeolitic imidazolate frameworks and application to CO_2 capture", *Science*, **319**, 939-943 (2008).
18. A. Torrisi, R. G. Bell, and C. Mellot-Draznieks, "Functionalized MOFs for enhanced CO_2 capture", *Cryst. Growth Des.*, **10**, 2839-2841 (2010).
19. A. Torrisi, C. Mellot-Draznieks, and R. G. Bell, "Impact of ligands on CO adsorption in metal-organic frameworks: First principles study of the interaction of CO with functionalized benzenes. II. Effect of polar and acidic substituents", *J. Chem. Phys.*, **132**, 044705 (2010).
20. S. Yang, X. Lin, W. Lewis, M. Suyetin, E. Bichoutskaia, J. E. Parker, C. C. Tang, D. R. Allan, P. J. Rizkallah, P. Hubberstey, N. R. Champness, K. M. Thomas, A. J. Blake, and M. Schröder, "A partially interpenetrated metal–organic framework for selective hysteretic sorption of carbon dioxide", *Nat. Mater.*, **11**, 710-716 (2012).
21. A. Bhattacharyya and C. M. Klapperich, "Mechanical and chemical analysis of plasma and ultraviolet–ozone surface treatments for thermal bonding of polymeric microfluidic devices", *Lab Chip*, **7**, 876-882 (2007).
22. A. Ganguly, S. Sharma, P. Papakonstantinou, and J. Hamilton, "Probing the thermal deoxygenation of GO using high-resolution in situ X-ray-based spectroscopies", *J. Phys. Chem. C*, **115**, 17009-17019 (2011).
23. G. T. Hefter and R. P. T. Tomkins, "The experimental determination of solubilities", Vol. 6, John Wiley and Sons, New York, NY (2003).

24. S. Gregg and K. S. W. Sing, “Adsorption, surface area, and porosity”, Academic Press, (1983).
25. G. Titelman, V. Gelman, S. Bron, R. Khalfin, Y. Cohen, and H. Bianco-Peled, “Characteristics and microstructure of aqueous colloidal dispersions of graphite oxide”, *Carbon*, **43**, 641-649 (2005).